

# Experimental investigation of exit dynamics of a circular cylinder out of water and silicone oil

Intesaaf Ashraf<sup>1</sup>, Lionel Vincent<sup>2</sup>, Romain Falla<sup>3</sup>, Jean-Philippe

Ponthot<sup>3</sup>, Vincent Terrapon<sup>3</sup>, Benoit Scheid<sup>2</sup>, and Stéphane Dorbolo<sup>1</sup>

<sup>1</sup> *PtYX, Département de Physique, Université de Liège (ULiège), 4000 Liège, BE*

<sup>2</sup> *Transfers, Interfaces and Processes (TIPs), Université Libre de Bruxelles (ULB), 1050 Brussels, BE*

<sup>3</sup> *Aerospace and Mechanical Engineering Department, Université de Liège (ULiège), Liège, BE*

(Dated: June 25, 2024)

Experimental investigations of the exit dynamics of a horizontal cylindrical object were performed in water and silicone oil (50 cSt). The fully immersed cylinder was initially at rest in a still fluid tank before being pushed (or pulled according to the measurement procedure) upwards at a constant velocity. The cylinder geometry was chosen to approach two-dimensional conditions in the transverse direction and, thus, allow comparison with two-dimensional numerical simulations. Firstly, we demonstrate that these conditions are better satisfied for a large aspect ratio cylinder equipped with vertical side plates. Secondly, the influence of the initial depth on the liquid entrained and the wake generated by the cylinder is discussed. It is shown that the wake destabilizes in the form of symmetry breaking in the case of water, while it remains symmetrical in the case of oil even for long travel in the bath. The deformation of the bath is found to be independent of the starting depth when the starting depth is larger than 6 times the cylinder diameter. In the present case, this criterion reflects also the finite acceleration of the cylinder to reach the determined constant exit velocity. Measurements in a range of exit speeds between 0.1 and 1 m/s indicate that the thickness of the liquid above the cylinder, when the cylinder starts crossing the interface, increases with the speed according to a logarithmic law of the Froude number. During the subsequent drainage, the evolution of the coated liquid thickness is found to first decrease exponentially with time just after the crossing of the interface. At later times, a change of regime occurs and the drainage follows the inverse of the square root of time irrespective of the crossing speed. Finally, the force necessary to maintain a constant exit speed during the motion of the cylinder inside and outside the bath is analyzed. This global measurement of the entrained liquid confirms the square root scaling of the thinning with time during the drainage process.

## I. INTRODUCTION

The physics of a body entering or exiting a liquid bath has been the subject of numerous studies, mostly driven in recent years by space (e.g., the splashdown of spacecraft), military (e.g., missile launching by submarines) and industrial (e.g., coating) applications. The water entry and exit problems are also commonly found in nature, for instance animals crossing the water-air interface [1]. While research on water entry has primarily focused on optimum design, shape, and entry velocity [2–7], water entrainment and subsequent drainage are of particular interest in the water exit problem [8]. In both cases, accurate experimental measurements, theoretical analysis and numerical simulations are challenging because of the complexity of the phenomena to take into account, such as interfacial physics and fluid-structure interactions [9–12].

The water exit problem can be categorized according to different aspects. The body motion can be forced through an imposed displacement [11, 13] or an external force [14], driven by buoyancy (when playing with balloon in a swimming pool [15]) [10] or a combination of an initial forced motion followed by an inertial phase [16]. Regarding the shape of the body, most works have focused on rather canonical shapes, including spheres [10, 11, 16, 17], vertical cylinders [13, 18], horizontal cylinders [8, 19, 20],

prolate ellipses [21], or even square cylinder [22].

The motivation to study the horizontal cylinder exit is to restrict the flow around the object to provide two-dimensional conditions for the flow around the section of the object. The water exit of a horizontal cylinder was first studied by [19]. Some inspiring experimental works can be found herein. A few years later, the same group [20] performed two-dimensional numerical simulations of the free-surface deformation of an initially calm water surface. In this paper, the experimental data set can be found for a “short” cylinder (the length being two or three times the diameter of the cylinder).

A more extensive work was performed by [12] including the case of the sphere. Both numerical simulations and some experimental results were presented. According to this work, two coefficients could be defined, namely the entering coefficient and the exit coefficient that result from the ratio between the pressure acting on the body and the Bernoulli pressure due to the motion. The cylinder whose aspect ratio (length divided by radius) was equal to 4, was equipped with vertical end-plates in order to keep a parallel velocity field to the direction of the motion. The measurements are compared to a model CIP (constrained Interpolation Profile) based on a work by [23] with a good agreement for a reduced set of imposed conditions. Besides, they carried out simulations at four different Froude numbers (defined as the square of the object speed divided by the gravity times the radius

of the object) i.e.  $Fr = 1.65, 4.12, 5.77$ , and  $8.24$ . Prior the cylinder starts crossing the interface, the free water elevation located above the cylinder could be measured. They observed that the free water surface elevation was strongly dependent upon the Froude number for values below  $4.12$ . However, for large speed (Froude number between  $4.12$  and  $8.24$ ), the surface elevation time dependence is nearly the same. Finally, they reported that waterfall breaking gets more intense as the Froude number increases due to the vortex generated in the wake. The waterfall reduces to a ligament at low speeds. The destabilization of the ligament and the coating thickness are reported numerically in a recent paper [24].

Regarding numerical simulations, in [14], the problem was numerically solved using a method based on VOF (volume of fluids). The motion was driven by applying a constant force and the considered starting depths were less than 3 times the cylinder diameter. On the other hand, both 2D and 3D simulations were performed. That allowed to determine the motion of the free interface (2D case) and to show some interesting dewetting phenomena (3D case) along the cylinder after the cylinder crossed the liquid interface. This dewetting could be observed in a case of a hydrophobic coated cylinder for example.

According to the applications, the fast drainage is required (missile, fishing birds) or, on the other hand, a slow drainage is demanded. Indeed, when an object has to be coated by a painting for example, the simplest way to proceed is to plunge the object in a large bath and to pull it out of the bath. The speed of pulling, the viscosity and the surface tension of the fluid, as well as the contact angle have to be taken into account for the coating of surface parallel to the pulling direction. This problem of the extraction of a solid from a liquid was addressed by Landau, Levich and Derjaguin (LLD) for viscous liquids and/or small velocities [25, 26]. The configuration is rather generic and is found in numerous industrial processes involving the dip-coating of a surface to transform its property (coloring, anti-scratching, anti-wetting, anti-oxidizing, etc...). Studies have shown the richness of the LLD problem by considering the effects on the liquid entrainment of complex fluids [27], solid micro-textures [28] and solid elasticity [29]. These researches improve the reliability and the control of the dip-coating process. Some works have considered the influence of the inclination, either of the substrate [30] or of the pulling direction [31] or even upside down [32], but the amount of liquid entrained by lifting a sphere (for example) out of a bath remains an open question [33]. After having entrained the liquid, the horizontal drainage can start. Indeed, liquid film drainage along flat or curved surfaces is another field that has extensively been studied since Reynolds seminal work [34] and is still very active [35, 36]. Finally, the drainage directly influence the dripping or not of the fluid on the bottom side of the object [37].

Experiments concerning the way the film has been formed between the exit of the object and the drainage

is needed. Regarding the previous research on basic objects, the complete dynamics of the drainage must start by studying the crossing and the quantity of liquid entrained by the object. The major problem of such a scheme is that the thickness of the liquid located above the cylinder spreads on at least 6 orders of magnitude from the initial state ( $\approx m$ ) to the complete drainage ( $\approx .1 \mu m$ ) around the object.

## II. FRAMEWORK

The present work aims to provide experimental data on the complete motion of a horizontal cylinder crossing the interface, including (i) the elevation of the fluid surface during the motion of the cylinder inside the bath, (ii) the crossing over, (iii) the entrainment of the fluid, and eventually the link with the drainage of the fluid around the cylinder. The experimental set-up and the choice of the cylinder aspect ratio were designed such as to approach a two-dimensional flow around the cylinder, namely invariant data regarding any translation along the axis of symmetry of the cylinder. This later requirement benefits to numerical simulations.

Two strategies were envisaged to clinch or to reach 2D conditions of the flow around the cylinder. The aspect ratio  $AR$  defined as the ratio between the length  $L$  and the radius  $a$  of the cylinder, can be increased in such a manner that the flow close to the ends of the cylinder influences less and less the experimental results. The second strategy consists of adding vertical end-plates to the cylinder to force the fluid to flow perpendicularly to the symmetry axis of the cylinder. Based on PIV measurements, we will show that a large  $AR$  and the vertical end-plates are required to obtain conditions as close as possible to 2D.

The starting depth  $d$  is a relevant parameter regarding the development of the cylinder wake. Particle Imaging Velocimetry (PIV) was performed to characterize the fluid motion before the crossing. We will show that the results are independent of the starting depth when  $d > 12a$  in the present experimental set-up.

In practice, using the most appropriate cylinder (largest  $AR$  with or without end-plates) and starting with a sufficient large depth, only one parameter is to be tuned: the imposed vertical speed  $U$  of the cylinder, reflected by the Froude number, defined by  $Fr = U^2/ga$ , where  $g$  is the acceleration due to gravity. Whereas, the Reynolds number is defined as  $Re = \frac{2Ua}{\nu}$ , where  $\nu$  is the kinematic viscosity of the fluid. The height of liquid above the cylinder, the local thickness and the force necessary to keep the speed constant were measured as a function of time and of the speed.

These measurements were performed for two fluids : the water and the silicone oil (50 cSt). The aim of studying such different liquids is double: to evidence the influence of the viscosity but also to challenge the dewetting around the cylinder. Indeed, with the water, the dewet-

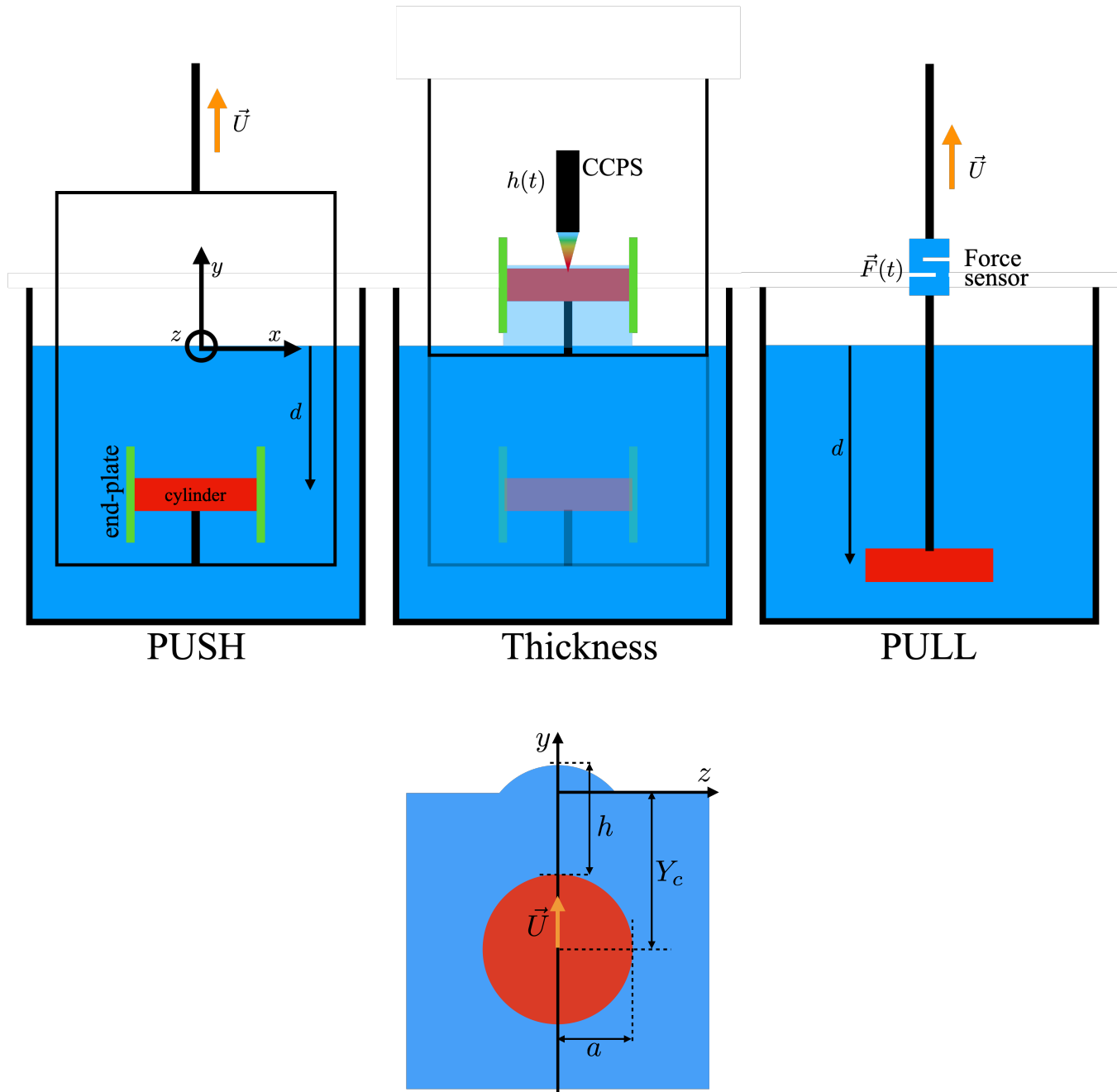


FIG. 1. (top) Schematic representations of the experimental configurations considered in this work. Push mode: the cylinder was attached by the bottom and pushed upwards via a light rigid frame. End-plates were added for some experiments to improve 2D conditions. Pull mode: the cylinder was attached by the top in order to limit the impact of the frame in the force measurements. Central panel: the cylinder can be stopped at a defined position to measure the oil film thickness evolution with time using a Chromatic Confocal Point Sensor (CCPS). (bottom) Sketch of the different parameters used in the work.

ting is very fast since the cylinder was made of metal. This is not the case for the oil since the slow drainage of the entrained fluid around the cylinder could be observed in a larger range of time.

The experimental setup is described in Sect. 3. The

different measured quantities during this study are there listed and presented. A typical experiment is presented to qualitatively describe the different regimes. The discussion about the experimental conditions and limitations is found in Sect. 4. The discussion concerns (i) the

size of the cylinder and how to reach the 2D conditions, and (ii) the influence of the starting depth on the results and on the wake. Important note: as already stated, we will show that the end plates (also named wings) and high aspect ratio ( $AR = 12$ ) cylinders are both required to reach 2D conditions. Consequently, all the experimental results presented in this paper, were obtained for the cylinder  $AR = 12$  equipped with wings. Two experiments were performed with different conditions, namely the film thickness direct measurements ( $AR = 10$  was used) and the force measurements ( $AR = 12$  was used but without end-plates). The reasons for these choices are given in the corresponding sections.

We present the deformation of the interface (Sect. 5) during the crossing. The upper position of the interface was recorded as a function of the position of the cylinder between an arbitrary starting time (when the top of the cylinder reaches the position of the interface at rest) and the crossing time (when the bottom of the cylinder reaches the position of the interface at rest). By image analysis, the maximum height reached by the air-fluid interface was detected as a function of the position of the cylinder during the motion. This allows defining and to analysing the thickness  $h$  of fluid ahead of the cylinder. The vertical speed of the cylinder was tuned between 0.1 and 1.0 m/s (Sect. 5.1). The final stage of the drainage was studied only in the case of the silicone oil using a Chromatic Confocal Point Sensor (CCPS, see Sect. 5.2). This sensor allows a direct measurement of  $h$  as a function of time. The CCPS was used only in the silicone oil case because the water dewets too fast on the aluminum cylinders, not allowing any meaningful measurements before drying.

While the cylinder was moving at an imposed constant speed, the force necessary to obtain this motion changes because of the time evolution of three elementary contributions: the drag, the buoyancy, and liquid entrainment. The force was measured (Sect. 6) as a function of the position of the cylinder (or, equivalently, as a function of time) and this, for speed  $U$  between 0.1 to 1.3 m/s. The cases of water and oil are compared for the largest considered aspect ratio in this work,  $AR = 12$ , for the best comparison to 2D conditions. End plates were not used due to their large influence on the force measurements. Global conclusions are drawn in Sect. 7.

### III. EXPERIMENTAL SET-UP

The experimental setup consisted of a large fluid tank fitted with a lifting system was used to pull or push the cylinder through the air-liquid interface. For the measurements, we used one or two synchronized high-speed cameras, a force sensor, a film thickness measurement device (CCPS) and a PIV system.

Figure 1(top) presents three different measurement configurations of the experimental set-up that are developed here below, namely the pushing mode (left), the

film measurement (center), and the pulling mode (right).

The fluid tank was made of glass in the case of water and of PVC in the case of silicone oil with dimensions of 78.5 cm x 27.5 cm x 72.5 cm for the length, the width and the height respectively. The lifting system was composed of a stage that moved along a linear guide. The motion was induced by a toothed belt entrained by a step motor. The cylinder under test for experiments was screwed to the stage via the carbon tube. The axis of symmetry of the cylinder was always oriented parallel to the fluid surface and was fixed on the moving frame by a rod that was screwed at one point of the symmetry plane of the cylinder.

The frame **pushed** the cylinder upwards so that the fluid surface could only be deformed by the top side of the cylinder. However, in the case of the force measurements, the cylinder was connected to the stage only using one carbon fiber tube and was **pulled** upwards instead of pushed. This allowed to reduce the influence of the frame (weight and liquid entrainment). To reach the constant speed set by the user, the acceleration was set to the maximum allowed by the motor, i.e. 4 m/s<sup>2</sup>. In so doing, the cylinder can cross the interface with a constant speed between 0.1 and 1.3 m/s. The experiments were carried out at a room temperature equal to  $20 \pm 2^\circ\text{C}$ .

The cylinder was made up of aluminium and had a smooth surface. Two types of cylinders were manufactured. One of the cylinder family had a radius  $a = 25$  mm for length between 25 and 250 mm corresponding to aspect ratios  $AR=1,2,4,6,10$ . Another one was with a radius  $a = 12.5$  mm offers the largest considered aspect ratio,  $AR=12$ . The end plates were added to the cylinder for some experiments (this is specified in the text). The end plates were 200 mm in diameter and 4 mm in thickness, and 150 mm for  $AR = 12$  for the same thickness.

The coordinate system ( $xyz$ ) is shown in Fig.1. The  $x$ -axis is oriented along the length of the tank, and the  $z$ -axis is along its width. The origin was set at the “at rest” free fluid-air interface considered as the horizontal plane of reference ( $xz$ ). The pushing/pulling  $Y$ -axis passes by the origin and is aligned with the vertical direction. The coordinate  $Y_c$  designates the vertical position of the center of mass of the cylinder. The coordinates  $y_c = Y_c/a$  are then normalized by the radius of the cylinder,  $a$ . The position  $y_c = 0$  is defined as the position of the cylinder for which the cylinder is half plunged in the bath (namely in the  $xz$  plane). Consequently,  $y_c = -1$  corresponds to the position when the top of the cylinder touches the fluid surface by the bottom; the cylinder is above the surface when  $y_c > 1$ .

Two of the controlled parameters in this study are the Froude number and the Reynolds number, which are varied by changing the cylinder exit velocity and the tank fluid viscosity. As assessed, two different kinds of fluids were used, i.e. water and silicone oil (50 cSt, PMX-200). The specific gravity of oil was 0.96 and kinematic viscosity was  $5.0 \cdot 10^{-5}$  m<sup>2</sup>/s at  $20^\circ\text{C}$ .

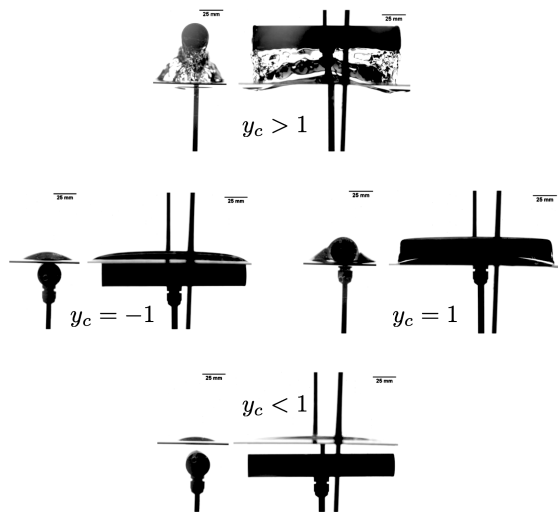


FIG. 2. Front and side views of the cylinder moving in the water and exiting the water surface for  $AR = 12$  at  $Fr = 8.2$ . The origin of time is  $t = 0$  s when  $y_c = 0$ . The different stages are (i) the motion in the fluid ( $y_c < -1$ ), (ii) the beginning of the crossing when  $y_c = -1$  and the end of crossing  $y_c = 1$ . The last stage (iii) is the drainage  $y_c > 1$ .

### A. Measurements

Different experimental techniques were used for the different stages of the cylinder.

*Particle velocimetry measurements* - A 2D planar PIV system was used for the flow investigation when the cylinder is still totally immerged. For the PIV exploration, the used LASER had a wavelength of 532 nm and peak power of 4 W and the seeding particles were  $\simeq 20 \mu\text{m}$  size. The open-source software PIVLab ([38]) post-processed the PIV images.

*Fluid surface deformation* - A white backlight (Efflux LED) was used to illuminate the cylinder and the fluid surface. Two high-speed M-310 phantom cameras acquired images at a rate of up to 3200 Hz. The cameras were perpendicular to the tank so that their fields of view allowed a complete visualization of the crossing. The air-fluid interface was set in the middle of the image to reduce the parallax and to allow the tracking of the interface position.

*Force measurements* - A strain gauge SCAIME K25 (20 N) measured the force acting on the cylinder during the whole motion (through the pool, through the interface and during the drainage). The gauge was calibrated using known weights. The data acquisition was performed using a datalogger (Picolog). The camera trigger signal was also recorded by the Picolog, which allowed the synchronization of the force measurements and the images captured by the camera. The contribution of the pulling rod was also measured in the absence of any cylinder to subtract the contribution of the rod and the entrained liquid to the force.

*Thinning of the film* - The drainage of the silicone oil located at the top of the cylinder was slow compared to that of the water. Indeed, in this latter case, the film breaks up and the dewetting is nearly instantaneous after the passage of the cylinder through the interface. On the other hand, the oil wets the cylinder. Once out of the bath, a Chromatic Confocal Point Sensor (CCPS, STIL, OPTIMA+) was used to record the thickness of the oil film located at the summit of the cylinder as a function of time. The measurement was achieved when the cylinder was at rest. Consequently, the cylinder must be stopped in the measurement range of the CCPS. Moreover, the deceleration must occur when the cylinder is far from the interface because we needed to ensure a constant speed during the whole crossing process. For the largest considered speed, the cylinder stops on a distance of approximately 27 cm. The cylinder was then stopped about 30 cm above the surface of the bath to allow the complete crossing of the cylinder before deceleration.

### B. Description of a typical experiment

A typical experiment began by positioning the cylinder at a desired initial position  $d$  in the tank. The initial position may vary for each set of experiments according to what was measured and to the presence or not of end plates. Ideally,  $d$  should be as deep as possible in order to ensure that the set-point speed was reached as deep as possible before hitting the surface. Once the cylinder settled, a latency time of 15 min was observed so that all the surface waves were damped.

Then, the cylinder was moved upward from its initial position at a constant acceleration  $\gamma$  of  $4 \text{ m/s}^2$  until reaching the desired speed  $U$ . Then, the upward movement continued at a constant speed. For example, for a speed of 1.0 m/s, the cylinder reached the maximal speed after moving 120 mm from its initial position.

When the cylinder moved upward at a constant speed the system passed through different stages. For example, Figure 2 shows the front view and side view at the three different stages of the exit dynamics of the cylinder in water ( $AR = 12$ ), the cylinder velocity was  $U = 1.0 \text{ m/s}$  and the Froude number was 8.2.

**Stage 1** starts when the cylinder is far below the surface, it moves without visibly disturbing the free surface. At a certain depth, the free surface starts deforming, it elevates and presents a bump-like profile (figure 2) until the cylinder starts crossing the interface. The thickness  $h(y_c(t))$  refers to the vertical distance between the top of the cylinder and the surface elevation at time  $t$ . That thickness can be tracked using high-speed cameras;  $h^* = h(y_c = -1)$  corresponds to the moment the top of the cylinder reaches the surface of the bath at rest. The flow inside the bath during the excursion of the cylinder was measured using PIV.

**Stage 2** is the crossing-over also called bulging regime. The crossing starts when the top of the cylinder reaches

the initial position of the free water-air interface (i.e.  $y_c = -1$ ) (figure 2). The time  $t = 0$  is set at the moment when the cylinder axis of symmetry crosses the interface ( $y_c = 0$ ). The thickness  $h^*$  is the height of the water-air interface measured from the reference plan when  $y_c = -1$  (figure 2). The crossing ends when the bottom of the cylinder reaches the initial position of the interface i.e.  $y_c = 1$ , and from that moment, the interface profile starts resembling the cylinder.

Finally, **Stage 3** is the drainage stage also known as waterfall breaking and then ligament fragmentation [24]. The drainage starts immediately after the cylinder top surface crosses the horizontal plane of reference. When the cylinder emerges out of the water, the liquid entrained by the front and by the rear of the cylinder forms a cascade (figure 2,  $y_c > 1$ ). This cascade continues until all the liquid is drained out.

#### IV. EXPERIMENTAL CONDITIONS AND LIMITATIONS

The 2D conditions have to be satisfied as much as possible in order to be as close as possible to 2D models. The PIV allows us to check whether the flow lines are parallel to the direction of the cylinder motion. To satisfy the 2D conditions, two strategies were envisaged: (i) to increase the aspect ratio and (ii) to add end-plates to force the flow to remain 2D by decreasing the side effects. The second question concern the starting depth. First, we have to account for the acceleration (deceleration) length to reach the constant velocity. Second, we have to characterize the wake of the cylinder (in water and in oil) according to the starting depth. Third, we are simply limited by the size of the bath.

##### A. 2D conditions: Aspect ratio

An interesting observable is  $h^*/a$ : the height reached by the fluid interface when the cylinder reaches the interface ( $y_c = -1$ ). The measurement of  $h^*/a$  is presented as a function of the Froude number for 6 cylinders whose aspect ratios spread between 1 and 12 (see Figure 3a) in the case of water; the radius  $a$  was kept constant at 25 mm. The height  $h^*/a$  increases with the speed of the cylinder, i.e. with the Froude number and with the aspect ratio  $AR$ . The observed behavior of the entrainment is in line with the observation of the 12, in which it was reported the waterfall breaking gets more intense with the increase in Froude number.

The data were fitted using logarithmic law  $h^*/a = A \ln(Fr) + B$  where  $A$  and  $B$  are fitting parameters [39]. The fitting parameters depend on the  $AR$  for  $A$  between 0.07 and 17 and for  $B$  between 0.32 and 0.60. The fits are the solid curves in Fig.3a.

The cylinder which aspect ratio is lower or equal to 10 has a radius of 25 mm. For this family of cylinders, we observed that the curves  $h^*/a(Fr)$  are closer and closer. Indeed, if we report the values of  $h^*/a$  for  $Fr=4$  as a function of the aspect ratio in Fig.3c, the red bullets (that correspond to cylinder with a radius equals to 25 mm) seems to saturate for large aspect ratios, as expected. One expects that for even larger aspect ratio, the curve  $h^*/a(Fr)$  would collapse. For comparison, the evolution of  $h^*/a$  is also presented as a function of the Froude number for the  $AR = 12$  cylinder with and without wings but with a radius of 12.5 mm; the pink and the light blue data point in Fig. 3a. Surprisingly, the curves are not close to the curve obtained for  $AR = 10$  despite the fact that a saturation regime was nearly reached in this later case. On the other hand, the curves  $h^*/a(Fr)$  are very close for the situations with or without end-plate. This shows the role of the end-plates even at large aspect ratio.

We also reported the values of  $h^*/a(Fr = 4)$  for  $AR = 12$  in Fig.3c. They are the blue square without end-plates and open square with. The values are about 1.2 times larger than for the cylinder  $AR = 10$ ,  $a = 25$  mm. We conclude that, in our experimental set-up, the radius of the cylinder does play a role despite the normalisation of  $h^*$ . Therefore, the dimension of the bath is questioned. Indeed, the ratio between the radius of the cylinder and the bath lateral side changes, or more exactly the ratio between the section surface of the cylinder and the surface of the bath. This lateral confinement seems responsible for the absolute value of the liquid elevation.

Starting from the basic fact that a high aspect ratio is necessary, we compared two large aspect ratio cylinders in the case of oil, both equipped with wings, namely the case of the cylinders  $AR = 12$  and  $AR = 10$ . The variation of the deformation  $h^*/a$  as a function of the Froude number for the silicone oil is reported in Figure 3b showing the same qualitative behaviours as for the case of water. We again find that the results depend on the cylinder radius because of the confinement effect. However, we observe that, by simply multiplied the results obtained for  $AR = 10$  by a factor 1.2, we obtain the results obtained for  $AR = 12$  (open circles in Fig.3b). On the whole, we essentially observe the largest aspect ratio is ideal and that the end-plates do play a role. On top of it, we observe that the absolute values of  $h^*/a$  change by a multiplicative factor when the radius of the cylinder is changed. The multiplicative factor is difficult to predict regarding the finite size of the bath. However, we found here that we doubled the radius to get a 1.2 factor on  $h^*/a$ .

##### B. 2D conditions: End-plates

In order to determine whether the flow around the cylinder equipped with end plates has a 2D characteristic, PIV measurements were performed. The most fa-

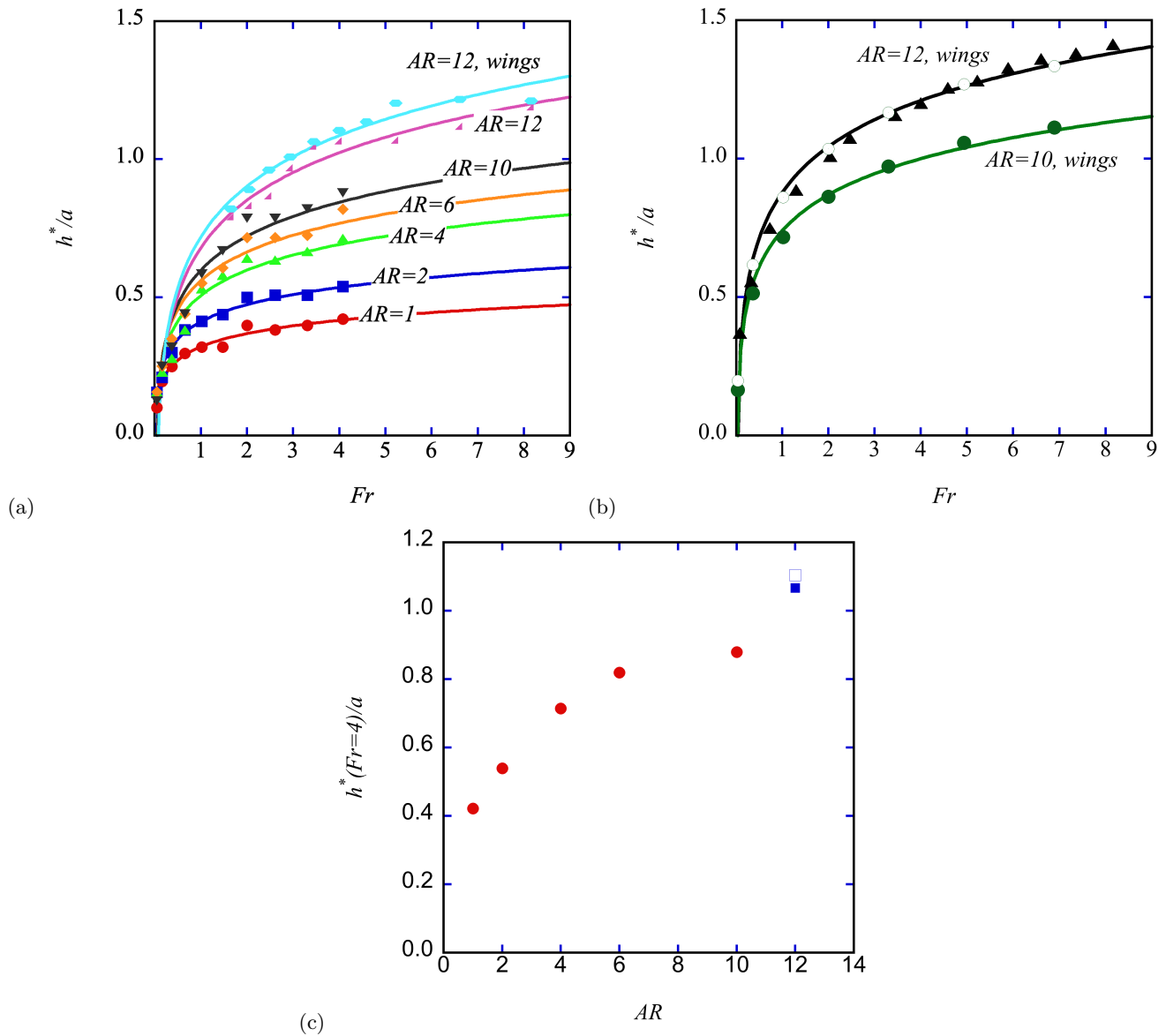


FIG. 3. (a) Water:  $h(y_c = -1)/a = h^*/a$  evolution as a function of the Froude number with  $d = 15a$ . The different symbols represent the average value of 7 experiments for different  $AR$  and the lines are logarithm fits (see text). (b) Silicone oil: Same plot as (a) but for comparing two aspect ratios: green bullets  $AR = 10$  ( $d = 15a$ ) and black triangles  $AR = 12$  ( $d = 32a$ ) equipped with end-plates. The open circles correspond to the results obtained for  $AR = 10$  multiplied by 1.2. (c) In the case of water,  $h^*/a$  for  $Fr=4$  extracted from Fig. 3(a) as a function of the aspect ratio. The red bullets correspond to cylinder  $a = 25$  mm and the blue squares to cylinders  $a = 12.5$  mm, the empty square is for the cylinder equipped with wings.

avorable aspect ratio was investigated namely  $AR = 12$ . The velocity field obtained by PIV is presented in Fig. 4a without end plates and with end plates in Fig. 4b. Without end plates, according to the PIV analysis, we observe that the flow in the middle of the cylinder is mostly parallel and straight at least until 2 cm from the extremities of the cylinder. The flow starts to exhibit a non-zero horizontal component while approaching the extremities of the cylinder. Consequently, the situation is not completely two-dimensional except close to the center of the cylinder.

In the case of the equipped end plates cylinder, the streamlines are parallel along the whole length of the cylinder as shown in Fig. 4b. The water located above the cylinder cannot escape by the lateral side. One can conclude that by using end plates, enhanced 2D conditions can be achieved.

In the following, end-plates were always used. The end plates were only removed for the force measurements. The weight of the end plates and the entrainment of the liquid by them biased the measurements.

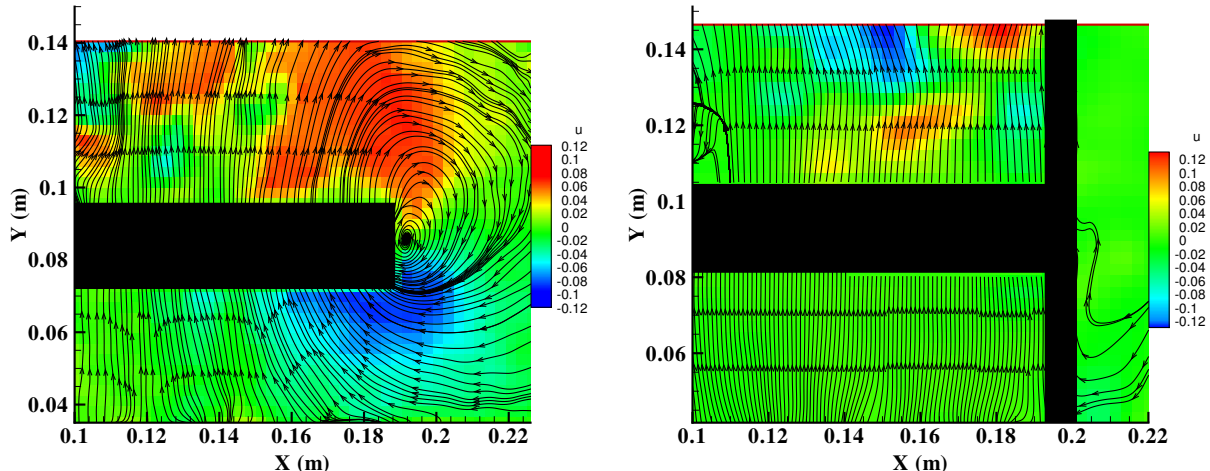


FIG. 4. Water case: (a) Flow field from the side of the cylinder at  $U = 0.5$  m/s and  $Fr = 2$  for the  $AR = 12$  without end-plates. (b) Flow field from the side of the cylinder with end plates. The color code is for the vorticity. The radius of the cylinder is 12.5 mm. The images show half of the cylinder that is 150 mm long.

### C. Starting depth

For the comparison between the motion in water and in oil, the cylinder with aspect ratio  $AR=12$  ( $a = 12.5$  mm) was released from depth  $d = 24a$ . The cylinder was equipped with end plates. Two typical speeds are here compared and correspond to Froude numbers  $Fr = 0.33$  and  $8.15$ . For the water, the Reynolds numbers are  $Re = 5000$  and  $Re = 25000$  respectively, while for the oil,  $Re = 100$  and  $Re = 500$  respectively. The results are shown in Figure 5. Figure 5a and Figure 5c correspond to the case of water and Figure 5b and Figure 5d to the case of silicone oil. The color represents the vorticity (the color scale is on the Figure legend).

In the case of water, vortex shedding occurs, and this is even at small Froude numbers. It can be seen from the figure that a pair of clockwise and anti-clockwise vortices are formed close to the cylinder. The vortices move along with the cylinder and are finally shed once the cylinder is out of the water. The strength of vortices increases with the increase in the Froude Number. The situation is completely different in the case of silicone oil. There is no vortex shedding at the release depth of  $24a$ . The wake remains symmetrical. The symmetry of the wake is important for any theoretical development. Indeed, it was shown that the evolution of the entrained liquid ahead of the cylinder is related to the presence of the wake [39]. Regarding the water, the symmetry breaking occurs even at small speeds ( $Fr = 0.33$ ). This influences both the entrainment and the collapse of the liquid behind the emerging cylinder. This situation contrasts with the silicone oil. In the most unfavorable sets of parameters, i.e. the highest speed and the deepest starting depth (Fig. 5d), the wake remains symmetrical. The volume of

liquid that is perturbed by the passage of the cylinder is rather well-defined compared to the case of water.

On the whole, the starting depth  $d$  does not influence the results concerning the deformation of the interface as soon as the depth is larger than a given value (3 times the diameter of the cylinder [13]). From the practical point of view, we observed that  $h$ ,  $h^*$  (and later the force measurement) were not found to depend upon the release depth any longer when  $d > 12a$ . This condition is stronger than the theoretical conditions but, we have to account for the acceleration phase of the cylinder. Therefore, the cylinder departing depth was set as deep as possible for each presented case. However, we indicate the starting depth in each case for record.

## V. MOTION OF THE INTERFACE

The evolution of the thickness  $h$  between the top of the cylinder and the air-fluid interface was measured as a function of the position of the cylinder  $y_c$  and this, for different speeds (pushing mode) between 0.1 and 1.0 m/s. The motion of the interface was obtained by determining the higher position reached by the liquid while the cylinder was moving. The optical axis of the camera was horizontal and contained in the interface plane. In so doing, the interface appeared in the middle of the image. Moreover, the camera was tilted by  $90^\circ$  in order to have a maximum of pixels along the vertical direction since the sensor had a 10:9 ratio.

Before the experiments, the cylinder was placed just under the interface and its position was recorded in order to determine the coordinate  $y_c = -1$  on the image. Then, two pictures of the cylinder were taken above and under the interface to obtain the calibration pixels to mil-



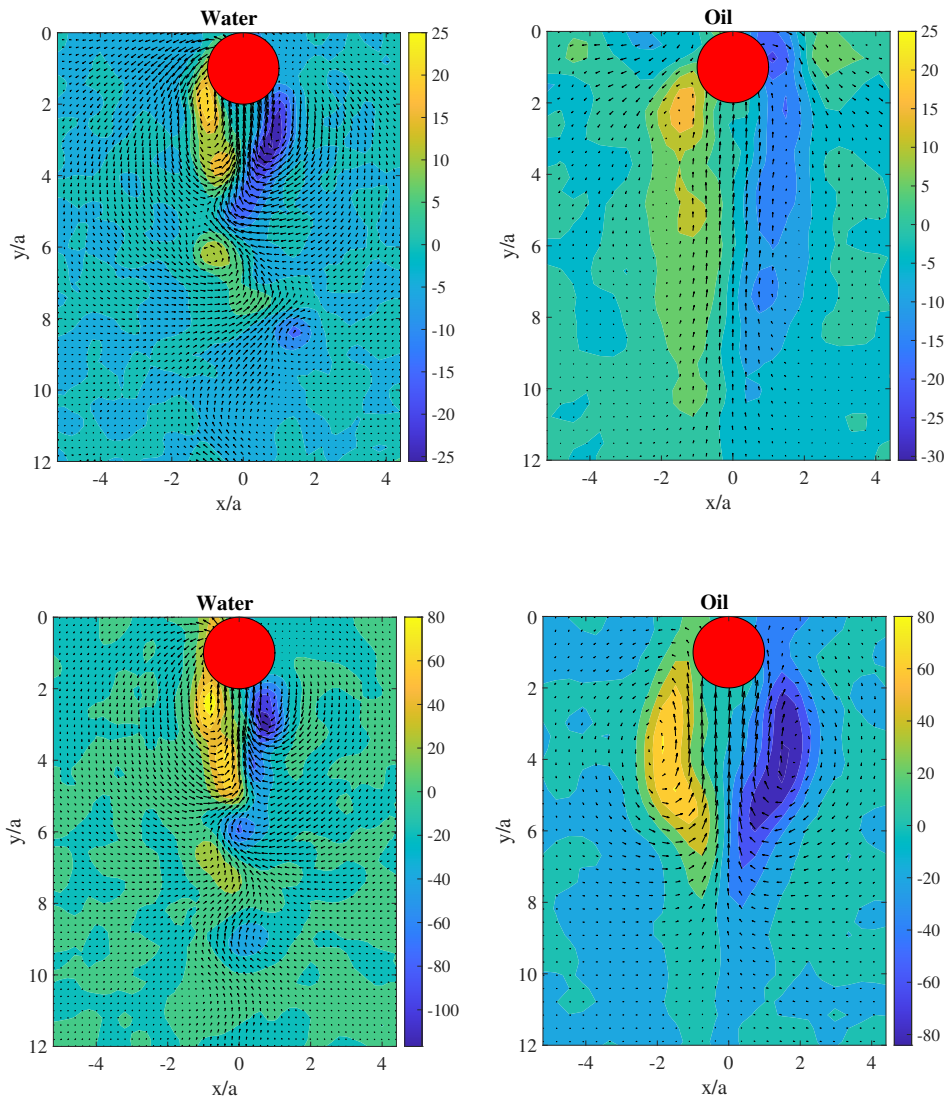


FIG. 5. The two graphics on the left (a) and (c) correspond to the case of water while the two on the right (b) and (d) correspond to the case of the silicone oil. The top line (a) and (b) are for  $Fr=0.33$  and the bottom (c) and (d) are for  $Fr=8.5$ . The released depth was  $d = 24a$  and the cylinder  $AR = 12$  was equipped with the end plates. The color code is for the vorticity.

limeters (which differs due to the water or oil refraction). The images were recorded close to the center of the cylinder to reach 2D conditions, even with the presence of end plates.

The contrast between the interface and the cylinder was sufficient to obtain the position of the interface and of the cylinder by subtracting an image of the background, i.e. in the absence of the cylinder. The image resulting from the subtraction was then thresholded. Note that the position of the cylinder was obtained by tracking the lower position of the cylinder; the higher position cannot be tracked as easily because of the interface deformation when the cylinder approaches the surface. In consequence, the position of the cylinder can only be

measured when the bottom part of the cylinder is located in the bath. The position  $y_c$  of the cylinder was then extrapolated based on the position of the cylinder before  $y_c = 0$ . The linearity  $y_c$  with time was checked and the slope allowed to confirm that the set-point speed was correct within a few percent.

In the case of silicone oil, the data  $h(y_c)$  can be completed over a long time thanks to the Chromatic Confocal Point Sensor (CCPS) sensor. Indeed, since the oil perfectly wets the cylinder, the entrained liquid slowly drained until reaching a thickness lower than  $10 \mu\text{m}$ . Synchronizing the data obtained by the CCPS with  $h(t)$  obtained by image analysis during the interface crossing, we can obtain the history of the film thinning over sev-

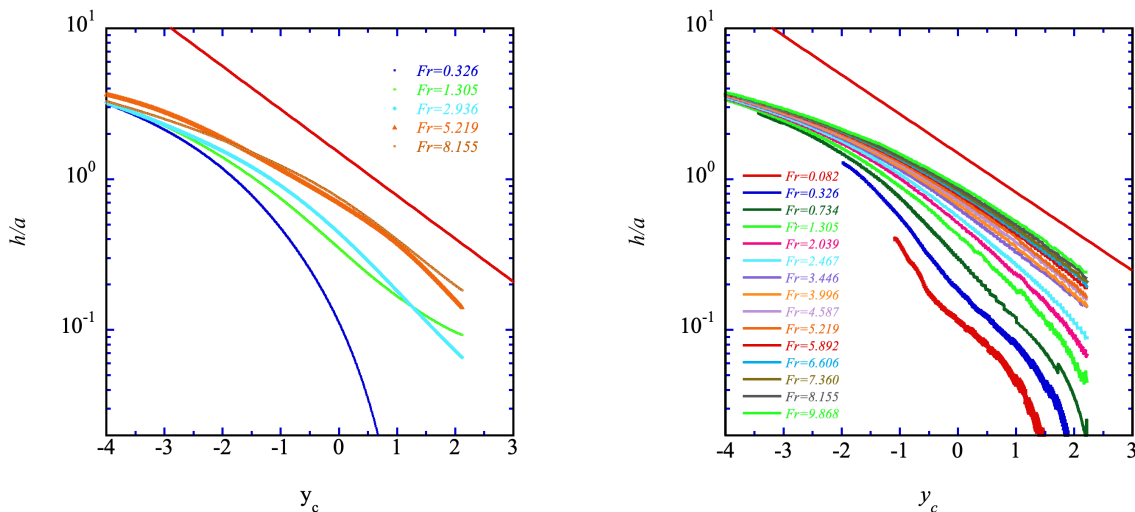


FIG. 6. Thickness of liquid  $h$  normalised by the radius  $a$  as a function of the position of the cylinder  $y_c$  for  $a = 12.5$  mm in (a) the case of **water** for  $d = 24a$  and (b) the case of **silicone oil** for  $d = 32a$ . The red lines correspond to an exponential decay function with  $\tau = 19$  ms; to convert the time into  $y_c$  units, the exponential functions were calculated for the higher  $Fr$  in both cases which correspond to  $U = 1.0$  m/s and 1.1 m/s in the case of the water and of the oil respectively.

eral decades of time. The synchronization was obtained by triggering the data logger with the same signal as the high-speed camera. The recorded images allow us to determine the time at which the cylinder crosses the interface.

#### A. Bulging stage ( $y_c < -1$ )

In Fig. 6a and 6b, we report the data  $h(y_c)$  for the water and for the oil respectively ( $AR = 12$  equipped with end-plates) in semi-log plots. Several speeds were tested between 0.1 m/s and 1.0 m/s as indicated in the legend through the Froude number. The starting depths were  $d = 24a$  and  $32a$  for the water case and for the silicone oil case respectively.

In both cases, the same behavior is observed. The fluid thickness ahead of the cylinder regularly decreases as the cylinder approaches the air-fluid interface  $y_c = 0$ . The decrease becomes more rapid when the cylinder comes as close as  $y_c = -2$  to the interface and crosses it. When the Froude number is high, the crossing of the interface is smoother and smoother because of the entrainment of the liquid. The curves tend to be closer and closer to each other. This convergence towards a limit curve is to be correlated with the observation of the values of  $h^*$  as a function of the Froude number  $Fr$ . That suggests that the decrease follows an exponential decay as a function of the position (as a function of time since  $y_c(t) = Ut$ ).

The exponential behavior can be understood according to a simple model. When the cylinder starts crossing

the interface, the liquid surrounds the cylinder as a layer with a thickness  $h$  which depends on the polar coordinate  $\theta$  (angle defined as the angle formed by the apex of the cylinder, the center of the cylinder and the position along the cylinder). The azimuthal speed  $v_\theta$  of the fluid at the apex of the cylinder ( $\theta = 0$ ) is zero and,  $v_\theta$  increases with  $\theta$ ; the maximum speed  $v_m$  is then found at  $\theta = \pi/2$ . The volume  $V$  of liquid located at the half top of the cylinder is then given by  $V = \pi a L h(\theta)$  and the flow rate  $\dot{V} = 2L h(\theta) v_\theta(\theta = \pi/2)$ . If the viscosity is neglected, the liquid is accelerated downwards by gravity and only the geometry of the flow is to be taken into account. We then find that  $\dot{h} \propto h$ , at first approximation, namely the thickness  $h$  experiences an exponential decay with time. The decay of  $h$  as a function of time was fitted by a decreasing exponential  $\exp(-t/\tau)$ . The red lines drawn in Figs.6 correspond to the function  $A_0 \exp(-y_c a / (U\tau))$  where  $A_0$  is an arbitrary constant and  $\tau$  is the characteristic time. The characteristic time was found to be 19 ms (in both water and oil cases) and the speeds used to draw the lines were chosen as the highest speeds represented in the Figure 6, namely  $U = 1.0$  m/s and  $U = 1.1$  m/s in the case of water and of oil respectively.

In addition, we can also inspect the origin of the characteristic time by estimating the escape speed of the fluid from the top of the cylinder. At first approximation, we may compute the time  $\tau_{fall}$  needed to fall from a height equal to the cylinder diameter:  $\tau_{fall} \approx \sqrt{2a/g} \simeq 50$  ms. Note that this approximation overestimates the typical time since the liquid can escape by both sides of the cylinder.

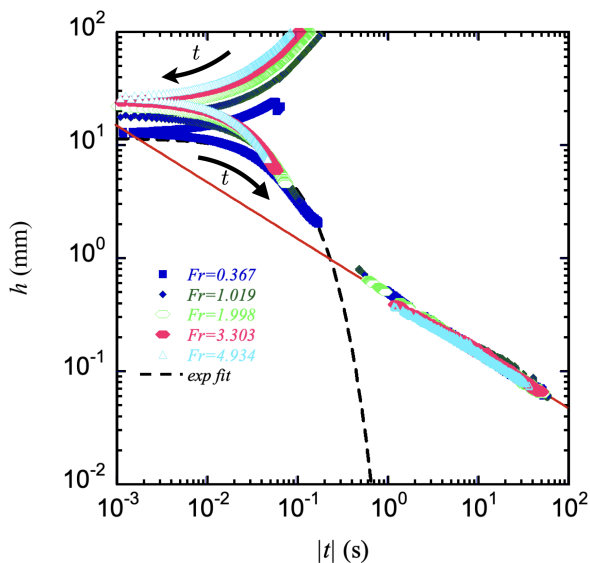


FIG. 7. (**Silicone oil**,  $AR = 10$ ) Evolution of the silicone oil thickness as a function of the absolute value of the time for different Froude numbers ( $d = 15a$ ). The data above  $h = 1$  mm are obtained using image analysis while the data below 1 mm are obtained using the CCPS. The arrows suggest the time direction. Both results from image analysis and from CCPS are presented (see text). The continuous red line is a fit  $t^{-1/2}$  of the data obtained with the CCPS. The dashed line is the fit of the data  $Fr = 0.367$  for  $t > 0$  by an exponential decay (see text).

### B. Drainage stage ( $y_c > -1$ )

When the cylinder is out of the liquid, the entrained liquid drains. This process depends on the wetting properties of the liquid on the cylinder material. The water dewets very quickly and the water film breaks as soon as the cylinder is above the surface. On the other hand, in the case of oil, the liquid flows down the top of the cylinder to the bottom forming a cascade back to the tank. The drainage time is much longer than in the case of the water for two reasons: (i) the oil wets the aluminium and (ii) the viscosity of the oil is 50 times higher than the viscosity of the water, the drainage time is increased consequently. Therefore, it is possible to directly measure the oil film thickness using a Chromic Confocal Point Sensor. For this purpose, the cylinder was stopped at a precise position such as the top of the cylinder was located in the measurement range of the CCPS. This range is as large as 1.3 mm. Then, the CCPS measured the film thickness as a function of time (acquisition frequency of 2500 Hz). Knowing the deceleration rate, the maximum speed reached by the cylinder, and the time at which the cylinder crosses the interface, we synchro-

nized the data obtained by image analysis and the direct thickness measurements. Contrary to the previous sections, we present the data for  $AR = 10$  equipped with end plates instead of  $AR = 12$ . The measurements using the CCPS are much more precise when the curvature radius of the cylinder is larger. Indeed, the pulling system allows it to stop at a precise position; however, because of vibrations and oscillations of the system, the lateral position induces some errors in the film thickness which are reduced for a large curvature radius as with the  $AR = 10$  cylinder. In Figure 7, both sets of data are presented as a function of time in a log-log plot. The range of thickness measurement and the range of considered time is large. The absolute time is presented such that  $h(|t|)$  are cusp curves; the upper part being the evolution of  $h(t)$  when  $t < 0$ . Then for  $t > 0$ , namely below the cusp point, the thickness decreases. The data for a time larger than 1 s were obtained thanks to the CCPS. The superposition of the data from the image analysis and from the CCPS allows us to obtain the variation of the liquid thickness over five decades of time and nearly four decades of thickness. The data from the CCPS are found to be the natural prolongation of the data obtained by image analysis. Moreover, regarding the drainage, the curves superpose showing that the drainage dynamics do not depend much on the initial conditions. The thin film of silicone oil drainage does not depend on the crossing speed  $U$ . This confirms the fact that the initial thickness at the top of an object that drains is not relevant. The red line in Fig. 7 is a fit of the CCPS data using a power law of the time,  $h \propto t^{-1/2}$  while the black dashed line is an exponential decay fit of  $h$  at the first instant after the interface crossing. A change of regime between the exponential decay and the power law occurs. The exponential decay (when  $t > 0$  is characterized by a typical time  $\tau = 93$  ms (in the case of the cylinder  $AR = 10$ ,  $\tau_{fall} \simeq 71$  ms). The regime change occurs at approximately when  $t \simeq 250$  ms and  $h \simeq 1$  mm. That change of regime reflects that the fluid viscosity becomes dominant when the film thins. Remarkably, whatever the crossing speed, the change of behavior occurs at the same time and for the same critical thickness.

## VI. FORCE MEASUREMENTS FOR WATER AND OIL EXPERIMENTS

The force measurements allow obtaining a global measurement from the start to the complete interface crossing. The force is the result of the cylinder weight, buoyancy, and drag force when the cylinder is below the surface. When the cylinder is out of the liquid, the buoyancy cancels and the liquid entrained contributes to the force. Moreover, the acceleration and the deceleration of the system are also present in the signal of the force as a function of time.

The evolution of the force is reported as a function of the cylinder position and this, for different pulling speeds.

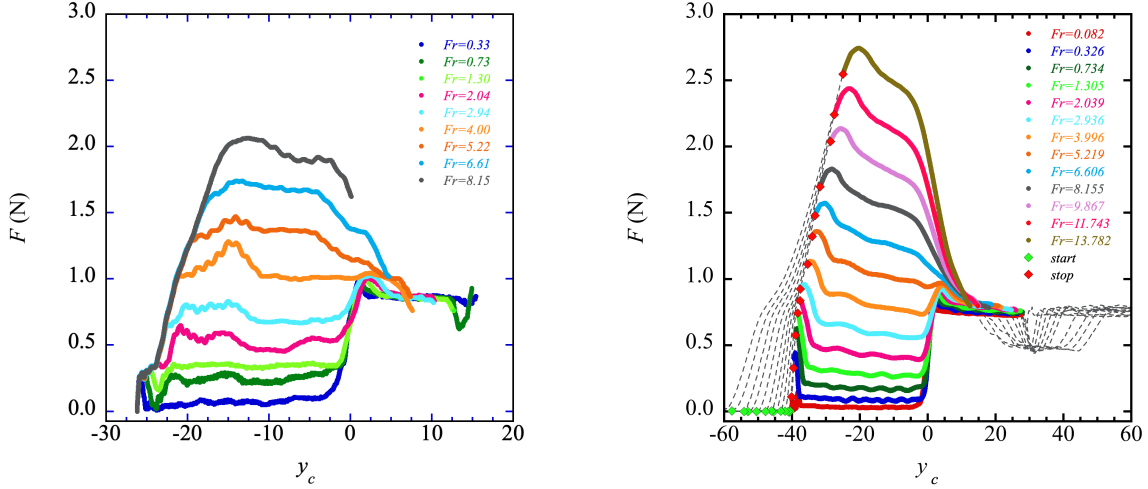


FIG. 8. (a) Water: Force as a function of  $y_c$  in the case of water for 9 values of the Froude number (see Legend). The starting depth was  $d = 24a$ . (b) Silicone oil: Force as a function of  $y_c$  for 13 different values of the Froude number. The starting distance for the data was  $d = 38a$ . The acceleration and deceleration phases are grey lines and do not correspond to the right  $y_c$  since during the acceleration  $Y_c \neq Ut$ . The acceleration starts and stops at the green and red diamonds respectively.

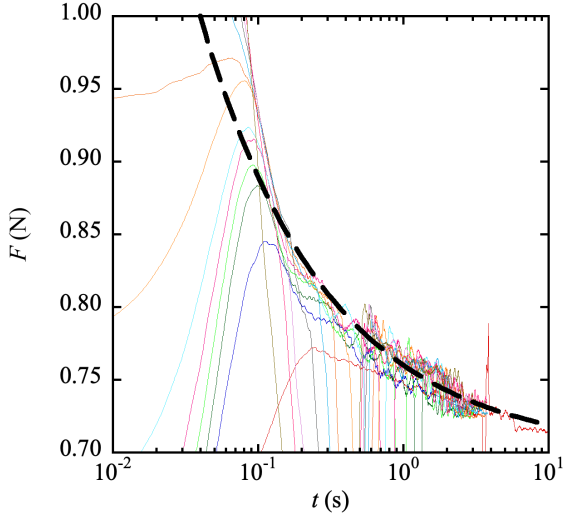


FIG. 9. Force as a function of time (same Legend as Fig.8b). The dashed curve represents a  $t^{-1/2}$  trend.

The aspect ratio used for these measurements was restricted to the highest considered value of 12 since the 2D conditions are the most satisfied when the cylinder is long. Note that the end plates cannot be used during the force measurement experiments because they can entrain

large quantities of oil (Landau-Levich pulling film along a vertical plane) and, in the case of water, generate waves at the surface of the water when crossing the interface (thus before the interface crossing).

Experimentally, the curve  $F(t)$  was obtained (this is Fig.9). The reference force  $F = 0$  N corresponds to the measured force when the cylinder is at rest and under the liquid surface. To compare the force measurements for the different considered speeds, the time series are converted into the position of the cylinder: a simple transformation following the rectilinear motion was operated, namely  $y_c = U(t)$ ,  $t = 0$  when the cylinder is located at  $y_c = 0$ . That means that, during the acceleration phase, the conversion  $t \rightarrow y_c$  following the linear law does not hold. However, we choose to present the curve including this bias in order to show the force variation during the complete motion of the cylinder.

In Figure 8a, the force  $F(y_c)$  is presented in the case of water and in Figure 8b in the case of silicone oil. In both cases, different speeds were considered as indicated in the Legend (Froude number). The data points corresponding to the acceleration and deceleration phases have been suppressed in the case of the water. In the case of oil, the acceleration phase is delimited by a green diamond when the acceleration stage starts and a red diamond when it ends. Both acceleration and deceleration phases are presented in grey dashed lines.

Regarding any force curves, we observed different stages. The force strongly increases during the acceleration stage (dashed line at low values of  $y_c$  for oil). The force reaches a maximum that is close to the end of the acceleration stage. Then the force starts dropping

before reaching a plateau representing the drag force of the liquid bath. Approaching  $y_c = -1$ , the force starts increasing again during the crossing since the buoyancy starts decreasing and since some liquid is entrained. This bump at around  $y_c = 1$  corresponds to the weight of the entrained water. Then the force decreased to the force corresponding to the weight  $F_0$  of the cylinder minus the buoyancy force.

When the set point speed is reached, regarding the evolution of the force inside the liquid ( $y_c < -1$ ), a plateau is observed. This is particularly observed at low Froude numbers: for  $Fr < 4$  in the case of the water and for  $Fr < 6$  in the case of silicone oil. The values of the plateaus  $F_d$  have been evaluated when the plateau is clearly visible. In both cases,  $F_d$  is found proportional to  $Fr$ . The dependence of the drag force  $F_d$  with the Froude number is compatible with a hydrodynamic force proportional to the square of the displacement speed  $U$ . This can be easily checked for the force measurements that exhibit a clear plateau.

For both the water and silicone oil cases, when the cylinder is close to the interface  $y_c \approx -1$ , there exists a particular Froude number beyond which the force exerted on the cylinder decreases at crossing instead of increasing due to the suppression of the buoyancy. For both the water and the silicone oil, the phenomenon occurs for  $Fr \approx 4$ . At this Froude number, the drag force plus the weight of the immersed cylinder is equal to the entrained liquid weight plus the weight of the emerged cylinder.

Finally, the force is reported as a function of time in Fig. 9 when the cylinder is out of the liquid in the case of oil, namely when  $t > 0$ . All the force measurements  $F(t)$  seem to converge towards a common curve. The dashed curve represents a power law, i.e.  $F \propto t^{-1/2}$ . The power law is compatible with the observed law of thickness decay found in Fig. 7 and with the common decay law found in the literature (see e.g. [35]).

## VII. CONCLUSION

In this paper, an experimental setup has been mounted in order to study the forced exit dynamics of a fully submerged cylinder. Two cases were considered: the water and the silicone oil (50 cSt) for Froude numbers lower than 15.

The aspect ratio of the cylinder has to be taken as large as possible and equipped with end plates to observe flow conditions as close as 2D conditions at the center of the cylinder. The best combination was checked by the PIV measurements and by the variation of the different parameters with respect to the aspect ratio. The starting depth was checked not to influence the results when in

practice  $d > 12a$ .

The wake of the cylinder was studied during the displacement of the cylinder in the bath. PIV measurements showed the formation of clockwise and anti-clockwise vortices during the cylinder upward movement. The vortices get easily diffused and are only observed in the vicinity of the cylinder. The vortices remain symmetrically positioned in the case of the silicone oil, and this is even for long-traveling cases ( $d > 20a$ ). In the case of water, the vortices are detached and asymmetrical.

The thickness of fluid ahead the cylinder was also measured according to two techniques: image analysis when the thickness is above 1 mm and Chromatic Confocal Point Sensor. The combination and the synchronization of both data allowed evidence of a change of regimes in the thinning of the entrained liquid at the apex of the cylinder. Just after the interface crossing, the thickness of the liquid decreases according to an exponential decay with time. For time larger than  $\simeq 250$  ms and thickness lower than  $\simeq 1$  mm, the thinning follows a scaling law, i.e.  $t^{-1/2}$ .

Finally, the force measurements carried on during the upward movement of the  $AR = 12$  cylinder allowed the estimation of the net drag force. Results showed the net drag force and entrained force increased with the cylinder upward velocity. The increase in drag force is obvious because as the velocity increases, the resistance to upward motion also increases. Consequently, there exists a particular Froude number beyond which the force drops after the passage of the interface. The force measurements also allow us to confirm the drainage dynamics according to the square root of the time.

More complex shaped objects should be studied regarding the total deformation of the interface. Indeed, while approaching the interface, the interface deforms according to a bump before revealing the shape of the object during the drainage stage. The force variations could also reveal the influence of the wake on the liquid entrainment. However, the speed of the crossing is confirmed to have a very small influence on the drainage dynamics of the fluid around the object.

## ACKNOWLEDGEMENTS

The financial support of the Belgian Fund for Scientific Research under research project WOLFLOW (F.R.S.-FNRS, PDR T.0021.18) is gratefully acknowledged. Part of the experimental setup was financed by *Fonds Spéciaux* from ULiège. SD and BS are FNRS senior research associates and research director respectively.

---

[1] B. Chang, J. Myeong, E. Viot, C. Clanet, H.-Y. Kim, and S. Jung, Jumping dynamics of aquatic animals, Jour-

nal of the Royal Society Interface **16**, 20190014 (2019).

- [2] R. Challa, S. C. Yim, V. Idichandy, and C. Vendhan, Rigid-object water-entry impact dynamics: Finite-element/smoothed particle hydrodynamics modeling and experimental validation, *Journal of Offshore Mechanics and Arctic Engineering* **136**, 031102 (2014).
- [3] R. Challa, V. Idichandy, C. Vendhan, and S. Yim, An experimental study on rigid-object water-entry impact and contact dynamics, in *ASME 2010 29th International Conference on Ocean, Offshore and Arctic Engineering* (American Society of Mechanical Engineers Digital Collection, 2010) pp. 383–391.
- [4] A. Mohtat, R. Challa, S. C. Yim, and C. Q. Judge, Numerical modeling of hydrodynamic impact and local slamming effects, in *Proceedings of the 13th International Conference on Fast Sea Transportation, Washington DC, Estados Unidos* (2015).
- [5] Q. Yang and W. Qiu, Numerical simulation of water impact for 2d and 3d bodies, *Ocean Engineering* **43**, 82 (2012).
- [6] V. V. Nair and S. Bhattacharyya, Water entry and exit of axisymmetric bodies by cfd approach, *Journal of Ocean Engineering and Science* **3**, 156 (2018).
- [7] B. Zhou, Z. Zhao, Q. Dai, W. Yao, X. Liu, Y. Zhang, A. Wang, and H. Zhang, Numerical study on the cavity dynamics of water entry and exit for a high-speed projectile crossing a wave, *Physics of Fluids* **36**, 063321 (2024), [https://pubs.aip.org/aip/pof/article-pdf/doi/10.1063/5.0212804/19991858/063321\\_1.5.0212804.pdf](https://pubs.aip.org/aip/pof/article-pdf/doi/10.1063/5.0212804/19991858/063321_1.5.0212804.pdf)
- [8] J. G. Telste, Inviscid flow about a cylinder rising to a free surface, *Journal of Fluid Mechanics* **182**, 149 (1987).
- [9] T. H. Havelock, The forces on a circular cylinder submerged in a uniform stream, *Proceedings of the royal society A* (1936).
- [10] T. T. Truscott, B. P. Epps, and R. H. Munns, Water exit dynamics of buoyant spheres, *Physical Review Fluids* **1**, 074501 (2016).
- [11] Q. Wu, B. Ni, X. Bai, B. Cui, and S. Sun, Experimental study on large deformation of free surface during water exit of a sphere, *Ocean Engineering* **140**, 369 (2017).
- [12] H. Haohao, S. Yanping, Y. Jianyang, C. Fu, and L. Tian, Numerical analysis of water exit for a sphere with constant velocity using the lattice boltzmann method, *Applied Ocean Research* **84**, 163 (2019).
- [13] P.-Y. Liju, R. Machane, and A. Cartellier, Surge effect during the water exit of an axisymmetric body traveling normal to a plane interface: experiments and bem simulation, *Experiments in fluids* **31**, 241 (2001).
- [14] S. Moshari, A. H. Nikseresht, and R. Mehryar, Numerical analysis of two and three dimensional buoyancy driven water-exit of a circular cylinder, *International Journal of Naval Architecture and Ocean Engineering* **6**, 219 (2014).
- [15] P. Bourrier, E. Guyon, and J. Jorre, The pop off effect: different regimes of a light ball in water, *European Journal of Physics* **5.4**, 225 (1984).
- [16] K. Takamura and T. Uchiyama, Effect of froude number on the motion of a spherical particle launched vertically upward in water, *Experimental Thermal and Fluid Science* **128**, 110453 (2021).
- [17] I. Ashraf and S. Dorbolo, Effect of the surface dimples on the exit dynamics of a sphere at a constant velocity, *Applied Ocean Research* **147**, 103996 (2024).
- [18] X.-s. Chu, K. Yan, Z. Wang, K. Zhang, G. Feng, and W.-q. Chen, Numerical simulation of water-exit of a cylinder with cavities, *Journal of Hydrodynamics, Ser. B* **22**, 877 (2010).
- [19] M. Greenhow and W.-M. Lin, *Nonlinear-free surface effects: experiments and theory*, Tech. Rep. (Massachusetts Inst Of Tech Cambridge Dept Of Ocean Engineering, 1983).
- [20] M. Greenhow and S. Moyo, Water entry and exit of horizontal circular cylinders, *Philosophical Transactions of the Royal Society of London. Series A: Mathematical, Physical and Engineering Sciences* **355**, 551 (1997).
- [21] B. Ni, A. Zhang, and G. Wu, Simulation of complete water exit of a fully-submerged body, *Journal of Fluids and Structures* **58**, 79 (2015).
- [22] I. Ashraf and S. Dorbolo, Exit dynamics of a square cylinder, *Ocean Engineering* **297**, 117106 (2024).
- [23] G. Miao, Hydrodynamic forces and dynamic responses of circular cylinders in wave zones, Ph.D. thesis, Dept. of Marine Hydrodynamics, NTH, Trondheim. (1989).
- [24] X. Wei, D. Li, J. Lei, J. Li, J. Riviero-Rodriguez, F. Lin, D. Wang, and B. Scheid, Exit dynamics of a sphere launched underneath a liquid bath surface, *Physical Review Fluids* **9**, 054003 (2024).
- [25] L. Landau and V. Levich, Dragging of a liquid by a moving plate, *Dynamics of Curved Fronts*, 141 (1988).
- [26] L. Landau and V. Levich, Dragging of a liquid by a moving plate, *Acta Physicochim. URSS* **17**, 42 (1942).
- [27] A. de Ryck and D. Quéré, Fluid coating from a polymer solution, *Langmuir* **14**, 1911 (1998).
- [28] J. Seiwert, C. Clanet, and D. Quéré, Coating of a textured solid, *Journal of Fluid Mechanics* **669**, 55 (2011).
- [29] H. Dixit and G. Homsy, The elastocapillary landau-levich problem, *Journal of Fluid Mechanics* **735**, 1 (2013).
- [30] E. Benilov, S. Chapman, J. McLeod, J. Ocknedon, and Z. V.S., On liquid films on an inclined, *Journal of Fluid Mechanics* **663**, 53 (2010).
- [31] S. Weinstein and K. Ruschak, Dip coating on a planar non-vertical substrate in the limit of negligible surface tension, *Chemical Engineering Science* **56**, 4957 (2001).
- [32] E. Jambon-Puillet, P. G. Ledda, F. Gallaire, and P. Brun, Drops on the underside of a slightly inclined wet substrate move too fast to grow, *Physical Review Letters* **127**, 044503 (2021).
- [33] M. Bhamla, C. Giacomini, C. Balemans, and G. Fuller, Influence of interfacial rheology on drainage from curved surfaces, *Soft Matter* **10**, 6917 (2014).
- [34] O. Reynolds, On the theory of lubrication and its application to mr beauchamp tower’s experiments, including an experimental determination of the viscosity of olive oil, *Philosophical Transactions of the Royal Society of London* **AI 77**, 157 (1886).
- [35] D. Chan and R. Horn, The drainage of thin liquid films between solid surfaces, *The Journal of Chemical Physics* **83**, 5311 (1985).
- [36] J. Coons, P. Halley, S. McGlashan, and T. Tran-Cong, A review of drainage and spontaneous rupture in free standing thin films with tangentially immobile interfaces, *Advances in Colloid and Interface Science* **105**, 3 (2003).
- [37] S. Eghbali, S. Djambrov, and F. Gallaire, Stability of a liquid layer draining around a horizontal cylinder: Interplay of capillary and gravity forces, *Physical Review Fluids* **9**, 063903 (2024).
- [38] W. Thielicke and E. Stamhuis, Pivlab—towards user-friendly, affordable and accurate digital particle image velocimetry in matlab, *Journal of open research software* **2** (2014).

- [39] L. Vincent, J. Rivero, R. Falla, A. Intesaaf, V. Terrapon, S. Dorbolo, and B. Scheid, Cylinder exit dynamics: inertial exit, and the effects of symmetric wake, containment and starting depth, preprint (2024).